Analytica Chimica Acta 753 (2012) 64–72

Contents lists available at SciVerse ScienceDirect

Analytica Chimica Acta

journal homepage: www.elsevier.com/locate/aca

Highly specific revelation of rat serum glycopeptidome by boronic acid-functionalized mesoporous silica

Liting Liu[a], Ying Zhang[b,*], Lei Zhang[b], Guoquan Yan[b], Jun Yao[b], Pengyuan Yang[b], Haojie Lu[a,*]

[a] Shanghai Cancer Center and Department of Chemistry, Fudan University, Shanghai 200032, PR China
[b] Institutes of Biomedical Sciences, Fudan University, Shanghai 200032, PR China

HIGHLIGHTS

- A highly ordered boronic acid-functionalized mesoporous silica was synthesized.
- The as-prepared material possessed both glycopeptide-suitable pore size and glycopeptide-specific selectivity.
- The as-prepared material showed highly efficient ability for enrichment of endogenous glycopeptides from serum.
- Rat serum glycopeptidome was revealed for the first time.

GRAPHICAL ABSTRACT

A highly ordered boronic acid-functionalized mesoporous silica was synthesized and applied for the revelation of rat serum glycopeptidome for the first time.

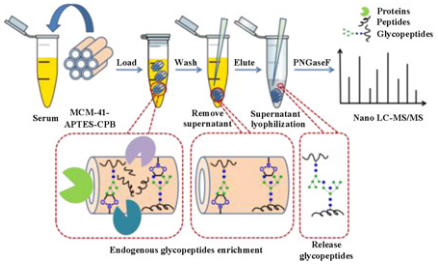

ARTICLE INFO

Article history:
Received 6 July 2012
Received in revised form
23 September 2012
Accepted 1 October 2012
Available online 9 October 2012

Keywords:
Serum glycopeptidome
Mesoporous materials
Size exclusion
Enrichment
Mass spectrometry

ABSTRACT

Although the specific profiling of endogenous glycopeptides in serum is highly inclined towards the discovery of disease biomarkers, studies on the endogenous glycopeptides (glycopeptidome) have never been conducted because of several factors. These factors include the high dynamic range of serum proteins, the inadequacy of traditional sample preparation techniques in proteomics for low-molecular-weight (LMW) proteins, and the relatively low abundances of glycopeptides. Boronic acid-functionalized mesoporous silica was synthesized in this study to overcome the limitations of the state-of-the-art methods for glycopeptidome research. The boronic acid-functionalized mesoporous silica exhibited excellent selectivity by analyzing glycopeptides in the mixture of glycopeptides/non-glycopeptides at molar ratio of 1:100, extreme sensitivity (the limit of detection was at the fmol level), good binding capacity (40 mg g^{-1}), as well as the high post-enrichment recovery of glycopeptides (up to 88.10%). The as-prepared material possessing both glycopeptide-suitable pore size and glycopeptide-specific selectivity has shown special capability for enriching the endogenous glycopeptides. Fifteen unique glycosylation sites mapped to 15 different endogenous glycopeptides were identified in rat serum. The established protocol revealed for the first time the rat serum glycopeptidome.

1. Introduction

Peptidome, the low-molecular-weight (LMW) subset of the proteome, has attracted increasing attention in recent years since it was first proposed in 2001 [1–4]. A serum sample is believed to contain these LMW circulating proteins and peptides, which can be rich sources of information [5–8]. The analysis of peptidome in biological samples via mass spectrometry (MS) potentially provides diagnostic and prognostic information on cancer and other diseases [9–11]. For example, an optimized, 12-member peptide ion thyroid cancer signature was developed by Villanueva et al., enabling classification of an independent validation set with 95% sensitivity and

* Corresponding authors. Tel.: +86 21 54237618; fax: +86 21 54237961.
E-mail addresses: ying@fudan.edu.cn (Y. Zhang), luhaojie@fudan.edu.cn (H. Lu).

0003-2670/$ – see front matter © 2012 Elsevier B.V. All rights reserved.
http://dx.doi.org/10.1016/j.aca.2012.10.002

95% specificity. However, only few reports on post-translational modifications of peptidome can be found although the awareness on the importance of the peptidome has greatly increased [12,13]. To date, more than half of the discovered cancer biomarkers are glycosylated proteins or peptides; the carbohydrate changes are closely related to the initiation and progression of tumors [14]. Therefore, the specific profiling of endogenous glycopeptides in serum and their glycosylated sites are highly inclined toward the discovery of disease biomarkers and clinical diagnosis.

Despite the potential of serum glycopeptidomics, some fundamental and serious barriers exist, hindering glycopeptidome research. First, the high dynamic range of serum proteins ($\sim 10^{12}$) renders the analysis of the human serum glycopeptidome a very challenging task [15]. Second, the molecular weight (MW) of the glycopeptidome is mostly lower than 20 kDa, which is similar to the peptidome, is difficult to be covered via traditional sample preparation techniques in proteomics. Lastly, glycopeptides usually exist at relatively low abundances (2–5%) compared with non-glycosylated peptides [16]. The glycan microheterogeneity further reduces the relative amount of glycopeptides and decreases the detection sensitivity. Therefore, a specific method to overcome the limitations of the traditional methods for glycopeptidome research needs to be developed.

Various sample pretreatment methods have been developed, including organic solvent precipitation [17], centrifugal ultrafiltration [18], solid phase extraction [19,20], and restricted-access materials based trap column [21,22], to cover the LMW range for peptidome research. Among these methods, mesoporous nanomaterials offer fresh approaches for addressing the fundamental barrier for the separation of peptidome because of their high enrichment capabilities based on a combination of adsorption and size-exclusion mechanisms [23,24]. The unique pore structures, rich surface properties, and extra-large surface areas of these mesoporous materials make them superior for peptide enrichment. However, they are insufficient for glycopeptidome research because sample pretreatment methods should be specific toward glycopeptides. Among the glycopeptide enrichment techniques, lectin affinity chromatography (LAC) is the most widely used, although different lectins have diverse affinities toward various carbohydrates [25–27]. Therefore, LAC has the limitation of capturing only a subset of the glycoproteome associated with the lectin epitope. The hydrazide-functionalized beads are another important technique that can efficiently capture glycopeptides through covalent bonding after the oxidation of the cis-diol groups of carbohydrates with periodate [28]. However, an additional oxidation step is needed, thereby increasing the experiment time and sample complexity. Other enrichment methods, for example, those based on the hydrophilicity of the glycan moiety [29,30] or the relative large size of glycopeptides [16], are of poor selectivity. Boronic acid-functionalized materials have been applied for the separation and detection of glycans or cis-diol compounds [31–37]. Recently, several boronic acid-functionalized nanoparticles for enriching glycopeptides have been developed to specifically capture glycopeptides [38–42]. Glycopeptides can be enriched with high selectivity and high efficiency based on the formation of a cyclic diester between boronic hydroxyl and 1,2-cis-diol on the glycan chain [43,44]. For example, mesoporous silica FDU-12 with a 5 nm pore entrance size was used as the matrix for grafting the boronic acid groups; this functional material showed good selectivity towards glycopeptides. FDU-12 possesses a cage-like, interconnected pore structure [45], which would allow for the entrapment of proteins with sizes close to (or slightly larger than) that of entrance pore, while minimizing protein leaching from the pores due to the restriction of the entrance pore [46], therefore, FDU-12 is usually used as an adsorbent for proteins and support for immobilizing enzymes [45–49]. However, this cage-like, interconnected pore structure of FDU-12 is not appropriate for the extraction of the peptidome because undesired proteins like some high abundance serum proteins (such as human serum album, 67 kDa, 5 nm × 7 nm × 7 nm) are simultaneously entering the pores. Therefore, all of these boronic-acid functionalized nanoparticles without the desired size-exclusion effect, as shown in both other works and our previous works [38–42], are still not applicable for glycopeptidome research. Mesoporous material with glycopeptide-suitable pore size and rich boronic acid groups would be the ideal material for glycopeptidome enrichment.

In this study, a highly ordered mesoporous silica MCM-41 with a small pore entrance size (2–3 nm) was functionalized with boronic acid groups. The attractive features of the prepared silica well met the requirements of serum glycopeptidome enrichment. Firstly, it has a small pore entrance size along with uniform mesopores so that high molecular weight (HMW) proteins are excluded from entering the pores. The size-exclusion ability was shown to exclude proteins with MWs larger than 12 kDa in standard protein mixtures. Secondly, abundant boronic acid groups were grafted on its internal surface; therefore, once the peptides and the LMW proteins enter the pores, the glycopeptides and the LMW glycoproteins can be selectively captured by the boronic acid groups. The excellent glycopeptide selectivity was demonstrated by analyzing glycopeptides in the digest mixture of horseradish peroxidase (HRP) and bovine serum albumin (BSA) with a molar ratio of 1:100. Thirdly, the combination of glycopeptide-suitable pore entrance size and glyco-selective effects of boronic acid groups possesses the size-exclusion ability to selectively capture the glycopeptides and the LMW glycoproteins from complex biological samples. Finally, a novel method for glycopeptidome research combined with glycopeptide enrichment by boronic acid-functionalized mesoporous silica and MS analysis was established. Rat serum glycopeptidome was revealed for the first time with 15 unique glycosylation sites mapped to 15 different endogenous glycopeptides identified.

2. Experimental

2.1. Materials

Mesostructured silica (MCM-41, hexagonal, particle sizes in the micron range), 3-aminopropyl-triethoxysilane (APTES, 99%), 4-carboxyphenylboronic acid (CPB), BSA, HRP, cytochrome c (Cyto C, 95%), myoglobin (Myo, 90%), soybean trypsin inhibitor (SBTI), 2,5-dihydroxy-benzoic acid (DHB, 98%) and ammonium bicarbonate (ABC, 99.5%) were obtained from Sigma–Aldrich (St. Louis, MO). N,N-dimethylformamide (DMF, 99.5%), 1-(3-dimethylaminopropyl)-3-ethylcarbodiimide hydrochloride (EDC, 99.0%), 1-hydroxybenzotrizole (HOBt, 99.0%), N-methylmorpholine (NMM, 98.0%), toluene (99.5%), hydrochloric acid (HCl, 36%) and triethylamine (TEA, 99.0%) were purchased from Sinopharm Chemical Reagent Co., Ltd. (Shanghai, China). PNGase F (95%) was obtained from New England Biolabs (Ipswich, MA). Acetonitrile (ACN, 99.9%, chromatographic grade), trifluoroacetic acid (TFA, 99.8%) and formic acid (FA, 96%) were purchased from Merck (Darmstadt, Germany). All these reagents were used as received without further purification except the toluene was dried by refluxing with sodium wire. Deionized water (18.4 MΩ cm) used for all experiments was obtained from a Milli-Q system (Millipore, Bedford, MA).

2.2. Preparation of rat serum sample

Rat blood sample was obtained from abdomen main artery of one rat. The sample was allowed to clot at room temperature (R.T.) for 1 h, followed by centrifugation at 1600 × *g* for 10 min at R.T. The

obtained supernatant (serum sample) was stored at −80 °C before analysis. The experiment was performed in compliance with the relevant laws and institutional guidelines. The experiment has been approved by the local authorities of Shanghai, China.

2.3. Preparation of boronic acid-functionalized MCM-41 silica

The boronic acid-functionalized MCM-41 silica was prepared using a three-step post-grafting method [50,51]. Firstly, MCM-41 was activated in HCl solution to obtain more hydroxyl groups. Typically, 200 mg of MCM-41 was mixed with 8 mL of 6 M HCl solution in a flask at R.T. for 10 h with stirring, followed by centrifugation. After the supernatant was discarded, the MCM-41 material was washed with deionized water several times until the pH of the supernatant was neutral. Secondly, the acidified MCM-41 was dried in vacuo at R.T. and continued to be dried in vacuo at 110 °C for 6 h. Next, APTES was introduced to prepare APTES bonded MCM-41 (denoted as MCM-41-APTES). 200 mg of the activated MCM-41 material was suspended in 60 mL of anhydrous toluene in a flask with stirring. The temperature was raised to 60 °C, and 0.4 mL of APTES was slowly added into the solution over 10 min with stirring. The mixture was stirred at 60 °C for 12 h under nitrogen (N_2). After that, the material was recovered and washed with toluene and ethanol three times, and finally dried in vacuo at 50 °C for 4 h. Lastly, CPB was introduced to prepare boronic acid-functionalized MCM-41 (denoted as MCM-41-APTES-CPB). 44 mg of CPB and 62 mg of HOBt were dissolved in 3.46 mL of DMF at R.T. After the solution was cooled to 0 °C in an ice-bath, 56 mg of EDC was added into the DMF solution and the mixture was maintained in the ice-bath for 15 min. 120 μL of NMM and 200 mg of MCM-41-APTES material were added into the above DMF solution and was gradually allowed to rise to R.T. The reaction solution was continuously vortexed for another 3 days at R.T. The resulting MCM-41-APTES-CPB was washed with DMF, water and methanol for further use.

2.4. Characterization

Transmission electronic microscopy (TEM) images were obtained with a JEOL 2011 microscope operated at 200 kV. Samples for TEM measurements were suspended in ethanol and supported on a carbon-coated copper grid. N_2 adsorption isotherms were measured using a Micromeritics Tristar 3000 analyzer at 77 K. Before measurements were taken, all samples were degassed at 393 K for more than 6 h. Fourier transform infrared (FT-IR) spectra were measured on a Nicolet Nexus 470 FT-IR spectrometer (USA). Thermogravimetric analyses (TGA) were monitored using a Mettler Toledo TGA-SDTA851 analyzer (Switzerland) from 25 to 800 °C under oxygen. Electrophoreses for protein separation were carried out by regular SDS-PAGE with 12% polyacrylamide gel and 5% stacking gel according to the manual introduction (Bio-Rad, USA).

2.5. Adsorption of standard proteins

Four standard proteins (HRP, SBTI, Myo and Cyto C) were dissolved in 10 mM sodium phosphate buffer (PBS) at pH 7.4 as a stock solution (0.2 mg mL^{-1}). To determine the quantity of adsorbed proteins, 16 μL of three materials (MCM-41, MCM-41-APTES and MCM-41-APTES-CPB) suspensions (10 μg μL^{-1} in PBS) were added into 100 μL of the stock solutions, respectively. Then, they were incubated with shaking for 2 h at R.T., followed by centrifugation at 14,000 rpm for 3 min. After the supernatants were decanted, 100 μL of 10 mM PBS solutions were used to wash the materials respectively (5 min at R.T.), followed by centrifugation (14,000 rpm for 3 min) to remove supernatants. Then 100 μL of the elution solutions (50% ACN with 0.1% TFA, pH 3) were added to elute the proteins from the three materials (30 min at R.T.). The supernatants collected in each step and 100 μL of the stock solutions (as the controls) were all lyophilized for SDS-PAGE analyses. The relative amounts of the proteins in supernatants before and after adsorption were compared by the difference in densities on the SDS-PAGE gel.

2.6. Enrichment of standard glycopeptides

Enrichments of standard glycopeptides from HRP were carried out from both peptide mixtures and rat serum samples. The incubation procedures differed but the washing and elution procedures remained the same. The incubation procedures were as following:

Enrichment of standard glycopeptides from peptide mixtures.

20 μL of MCM-41-APTES-CPB suspension (10 μg μL^{-1}) was added into 1.0 mL of the tryptic HRP and BSA mixture (67% ACN with 0.2% TEA, pH 8) with the HRP at a concentration of 25 nM and the BSA at a concentration of 2.5 μM, followed by incubation for 1 h at R.T. and centrifugation at 14,000 rpm for 5 min.

Enrichment of standard glycopeptides from serum.

A 5.0 μL serum sample was diluted with 20 μL of tryptic HRP solution (100 ng μL^{-1}), and then 50 μL ACN was added. The mixture was then heated in boiling water for 10 min and vortexed at 1500 rpm for 30 min. After being centrifuged at 12,000 rpm for 15 min at 4 °C, the supernatant was isolated. 0.2 μL of TEA and 20 μL of MCM-41-APTES-CPB suspension (10 μg μL^{-1}, 67% ACN) were added into the obtained supernatant and incubated for 1 h at R.T., followed by centrifugation at 14,000 rpm for 5 min.

The washing and elution procedures were both as follows: after the supernatant was decanted, 200 μL of 67% ACN with 0.2% TEA (pH 8) was used to wash the material (5 min at R.T.) twice. Then 6.0 μL of the elution solution (50% ACN with 1% TFA, pH 3) was added to release the glycopeptides from MCM-41-APTES-CPB (30 min at R.T.).

2.7. The binding capacity of boronic acid-functionalized MCM-41 silica for glycopeptides

To investigate the binding capacity, equivalent amounts (50 μg) of MCM-41-APTES-CPB were incubated with 1.0 mL of each tryptic HRP solution at different concentrations for 1 h. Then, the materials were decanted by centrifugation at 14,000 rpm for 5 min and these supernatants were analyzed by matrix-assisted laser desorption/ionization-time of flight mass spectroscopy (MALDI-TOF MS). The glycopeptides could only be detected when the total amount of HRP was higher than the binding capacity of the material; thus, the binding capacity of this material could be estimated according to the minimum detected signals of glycopeptides.

2.8. Enrichment of endogenous glycopeptides in rat serum

The rat serum was thawed on wet ice, and 1.0 mL of serum sample was slowly dropped into 2.0 mL of ACN at 4 °C. The mixture was immediately stirred and then heated in boiling water for 10 min, followed by vortexing at 1500 rpm for 30 min at 4 °C. After, the mixture was centrifuged at 12,000 rpm for 15 min at 4 °C, and then the supernatant was collected. 6.0 μL of TEA and 100 μL of MCM-41-APTES-CPB suspension (100 μg μL^{-1} in 67% ACN) were added into the obtained supernatant, and the resulting solution was incubated for 3 h at 4 °C, followed by centrifugation at 14,000 rpm for 5 min. After the supernatant was decanted, 400 μL of 67% ACN with 0.2% TEA (pH 8) was used to wash the MCM-41-APTES-CPB (5 min at R.T.) twice. Then 200 μL of the elution solution (20% ACN with 1% TFA) was added to release the glycopeptides from MCM-41-APTES-CPB (30 min at R.T.). After centrifugation (14,000 rpm for 5 min), 200 μL of the elution solutions with higher ACN concentrations (50% ACN with 1% TFA, 80% ACN with 1% TFA) were added to repeat the release steps in turn. The combined eluted portions

were lyophilized in vacuo and redissolved in 200 μL of 25 mM ABC. 1.0 μL of PNGase F was added under the instructions from the manufacturer and incubated at 37 °C for 12 h in order to detach the glycans.

2.9. MALDI MS analysis

Standard glycopeptides analyses were performed with MALDI MS. After centrifugation, 2.5 μL of elute was spotted on the MALDI plate and dried in the air. Then, 2.5 μL of matrix (12 mg mL^{-1} DHB dissolved in 50% ACN with 0.1% TFA) was also spotted on the MALDI plate and dried in the air for MS analysis. All mass spectra were acquired by a MALDI AXIMA QIT (Shimadzu Biotech, Japan). All measurements were carried out in reflector positive-ion mode with delayed ion extraction. Each sample and each MS run were performed at least 3 times in our experiments.

2.10. 1D nano-flow liquid chromatography-tandem MS (LC–MS/MS) analysis

Glycopeptides enriched from rat serum were analyzed by 1D nano-flow LC–MS/MS. The deglycosylated peptide solutions were lyophilized using a vacuum centrifuge and redispersed with 20 μL of 5% ACN containing 0.1% FA. Nano-LC–MS/MS experiment was performed on an HPLC system composed by two LC-20AD nano-flow LC pumps, an SIL-20 AC auto-sampler and an LC-20AB micro-flow LC pump (all Shimadzu, Tokyo, Japan) connected to an LTQ-Orbitrap mass spectrometer (Thermo Fisher, San Jose, CA). Sample was loaded onto a CAPTRAP column (0.5 mm × 2 mm, MICHROM Bioresources, Auburn, CA) in 4 min at a flow rate of 20 μL min^{-1}. The sample was subsequently separated by a C_{18} reverse-phase column (0.1 mm × 150 mm, packed with 3 μm Magic C_{18}-AQ particles, MICHROM Bioresources, Auburn CA) at a flow rate of 500 nL min^{-1}. The mobile phases were 2% ACN with 0.1% FA (phase A and the loading phase) and 95% ACN with 0.1% FA (phase B). A 90 min linear gradient from 2 to 45% phase B was employed. The separated sample was introduced into the mass spectrometer via an ADVANCE 30 μm silica tip (MICHROM Bioresources, Auburn, CA). The spray voltage was set at 1.6 kV and the heated capillary at 180 °C. The mass spectrometer was operated in data-dependent mode and each cycle of duty consisted one full-MS survey scan at the mass range 350–1500 Da with resolution power of 1,00,000 using the Orbitrap section, followed by MS/MS experiments for 15 strongest peaks using the LTQ section. The AGC expectation during full-MS and MS/MS were 10,00,000 and 10,000, respectively. Peptides were fragmented in the LTQ section using collision-induced dissociation (CID) with "wideband" function enabled and the normalized collision energy value set at 35%. Only 2+ and 3+ peaks were selected for MS/MS run and previously fragmented peptides were excluded for 90 s.

2.11. Database searching

All the MS/MS spectra in raw files were converted to single *.mgf files using MassMatrix Mass Spectrometric Data File Conversion Tools (version 3.9, http://www.massmatrix.net/download). Then, the *.mgf files were searched against the National Center for Biotechnology Information (NCBI) rat database (version 20111011, 113333 entries) using Mascot Version 2.3.0 (Matrix Science) followed by manual verification (described below) [52]. Peptides were searched using no cleavage enzymes specified, and variable modifications of Acetyl (Protein N-term) with the addition of 42.0106 Da, Met-oxide with the addition of 15.9949 Da, and Deamidation (N) with the addition of 0.98402 Da. Manual verification of the Mascot results considered the following criteria: the mass tolerances were 20 ppm for parent masses and 1.0 Da for fragment masses; the Mascot result had to represent the top score of all possible hits, with at least 5 b- and/or y-ions identified; and >80% of the major fragment ions observed had to match predicted fragments.

3. Results and discussion

3.1. Synthesis and morphology of boronic acid-functionalized MCM-41 silica

The boronic acid-functionalized MCM-41 silica was synthesized by a post-grafting method illustrated in Scheme 1(a). First, more hydroxyl groups were obtained by soaking MCM-41 in the HCl solution for 10 h. Mettalic and non-metallic impurities that adsorbed on the surface of MCM-41 were washed off and some Si—O bonds were opened by interacting with HCl. Then, the acidified MCM-41 was dried in vacuo at 110 °C for 6 h to activate the hydroxyl groups on the surface of MCM-41, and consequently, facilitate the following coupling of APTES. Next, APTES was coupled to the surface of MCM-41 in dry toluene under N_2. MCM-41-APTES was synthesized in organic solvent while the previously mentioned boronic acid-functionalized FDU-12 mesoporous silica was synthesized in aqueous solution. Although the original morphology of mesoporous structures can be maintained utilizing either solution, silane coupling agent was grafted onto the internal surfaces of the mesoporous structures as a monolayer while minimizing hydrolysis in the organic phase. More boronic acid groups can be grafted and the mesoporous structures would not be blocked by the aggregated oligomers of the hydrolyzed silanes. Finally, CPB was grafted onto the surface of MCM-41-APTES by amido bonds to obtain boronic acid-functionalized MCM-41. The boronic acid group has a specific recognition for the cis-diol of the glyco-structure. The obtained MCM-41-APTES-CPB could be recovered by centrifugation and redispersed by vortex. The TEM images of MCM-41, MCM-41-APTES and MCM-41-APTES-CPB are shown in Fig. 1(a)–(c). Fig. 1(c) reveals that MCM-41-APTES-CPB still maintains the well-ordered hexagonal pore structure as its unmodified counterpart MCM-41.

3.2. Characterization of materials

The synthesized MCM-41-APTES-CPB was characterized by different techniques. FT-IR spectra of the MCM-41, MCM-41-APTES, MCM-41-APTES-CPB were compared in Fig. 2(a). The vibrations (2928, 2854, 1457, and 796 cm^{-1}) shown in the IR spectra. Fig. 2(a) contributed by methylene groups demonstrate the successful functionalization of APTES on MCM-41. The dramatic intensity loss of the band at 957 cm^{-1} is ascribed to the scissor bending vibration of the Si–OH bonds after the APTES grafting, and also indicates that the surface of the MCM-41 material has been modified by APTES. The appearance of bands at 1535 cm^{-1} and 1390 cm^{-1} due to the vibrations of benzene rings and B—O bonds clearly proves that boronic acid-functionalized mesoporous silica has been obtained.

TGA was performed to estimate the relative composition of MCM-41 and the grafted organic layers. As shown in Fig. 2(b), MCM-41-APTES and MCM-41-APTES-CPB displayed distinct mass-loss profiles above 250 °C compared to that obtained in the MCM-41. MCM-41-APTES revealed a slightly high organic mass release of 10–11 wt.% from 400 °C to 800 °C which was attributed to the weight loss of grafted APTES. Differing from curve B, the prepared MCM-41-APTES-CBA by a post-grafting process (curve C) could be responsible for the weight loss of both APTES and CPB, and the mass release was of ~5 wt% between 250 °C and 400 °C was attributed to the weight loss of grafted CPB. The weight loss in the total amount of the grafted organics in MCM-41-APTES and MCM-41-APTES-CPB were 11.2 wt% and 16.2 wt%. Correspondingly, the N and B concentrations were estimated to be 50.51×10^{-5}

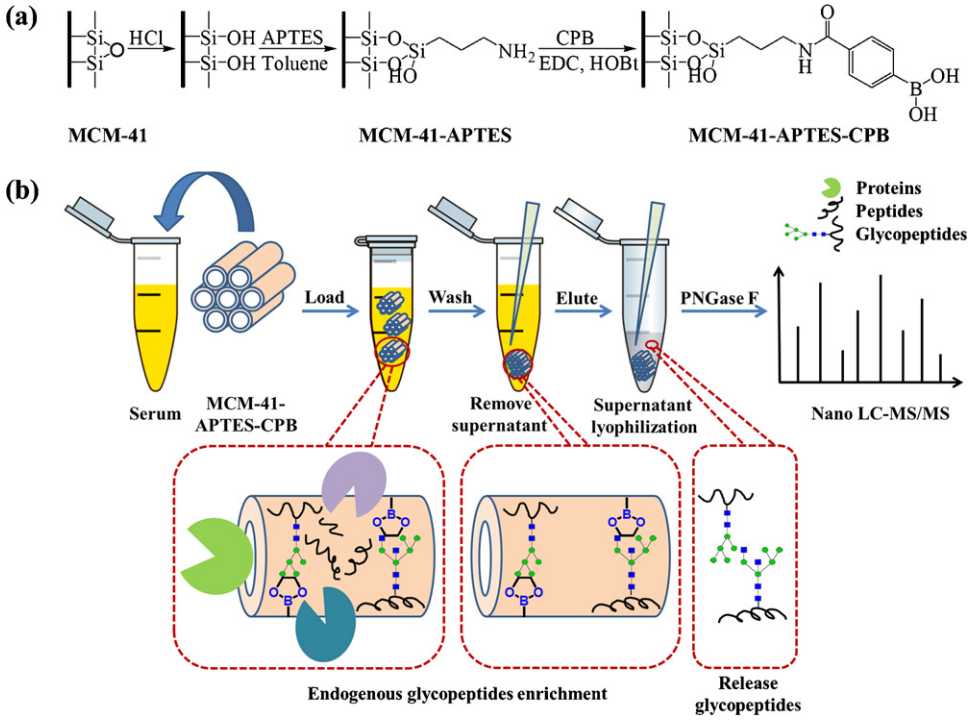

Scheme 1. (a) Schematic overview of the preparation of boronic acid-functionalized MCM-41 mesoporous silica; (b) flowchart of the enrichment of endogenous glycopeptides in rat serum followed by nano-LC–MS/MS detection.

and 33.56×10^{-5} mol g^{-1}, respectively. The content of boron of the as-prepared material was 0.4 wt%, which was not far from the value 0.8 wt% of the previous reported boronic acid functionalized SnO_2@Poly(HEMA-co-St-co-VPBA) core-shell nanoparticles [39]. Because the SnO_2@Poly(HEMA-co-St-co-VPBA) nanoparticles were synthesized by means of a hydroxyl-exchange reaction and a polymerization route, a very large amount of boronic acid can be introduced in such a polymerization process. But the as-prepared MCM-41-APTES-CPB was based on grafting the boronic acid on the silica matrix MCM-41, which afforded relative limited grafted sites. Therefore, the amount of boronic acid was less than that on SnO_2@Poly(HEMA-co-St-co-VPBA) nanoparticles. The content of boron was also measured by inductively coupled plasma-atomic emission spectrometry (ICP-AES), and the B concentration was estimated to be 14.54×10^{-5} mol g^{-1}, which slightly differed from TGA results.

3.3. Size-exclusion effect of MCM-41-APTES-CPB

To confirm the size-exclusion effect of MCM-41-APTES-CPB, its performance was evaluated using a mixture of four standard proteins with different sizes (see supporting information, Table S1). The SDS-PAGE results (Fig. 3) show that smaller proteins, such as Myo and Cyto C enter the pores of MCM-41 (lane 4), whereas bigger proteins, such as HRP and SBTI are excluded from the pores (lane 2). Moreover, the MW cutoff effect of pristine MCM-41 is consistent with previous reports [23]. All four standard proteins could not enter the pores (lanes 8 and 12), and they remain in the solution (lanes 6 and 10) after the post-grafting of APTES and APTES-CPB. The pore sizes of the modified MCM-41 materials are assumed to decrease with increased modified organic layers. Consequently, these proteins are excluded from the pores. The N_2 adsorption measurement confirmed the hypothesis of the current study (see

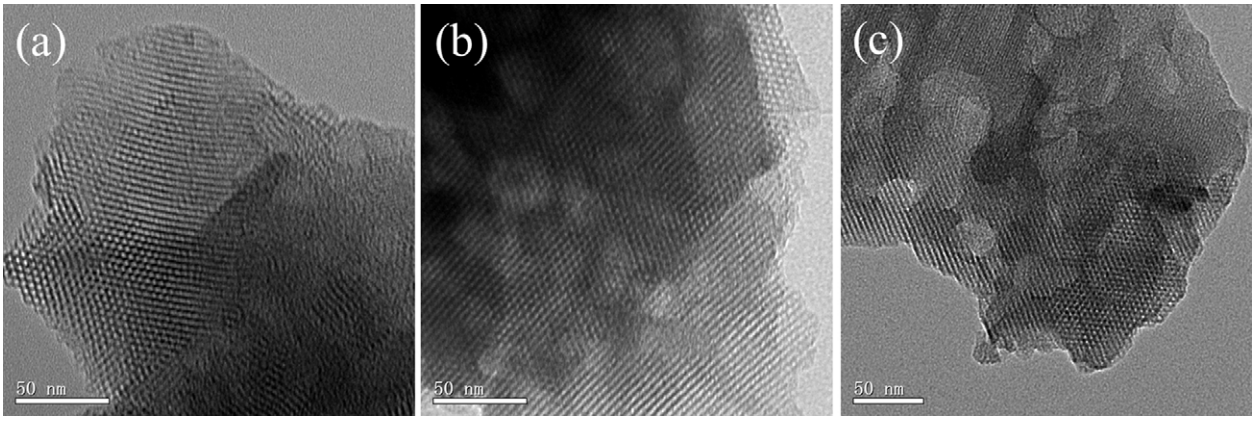

Fig. 1. TEM images of the synthesized (a) MCM-41, (b) MCM-41-APTES, and (c) MCM-41-APTES-CPB.

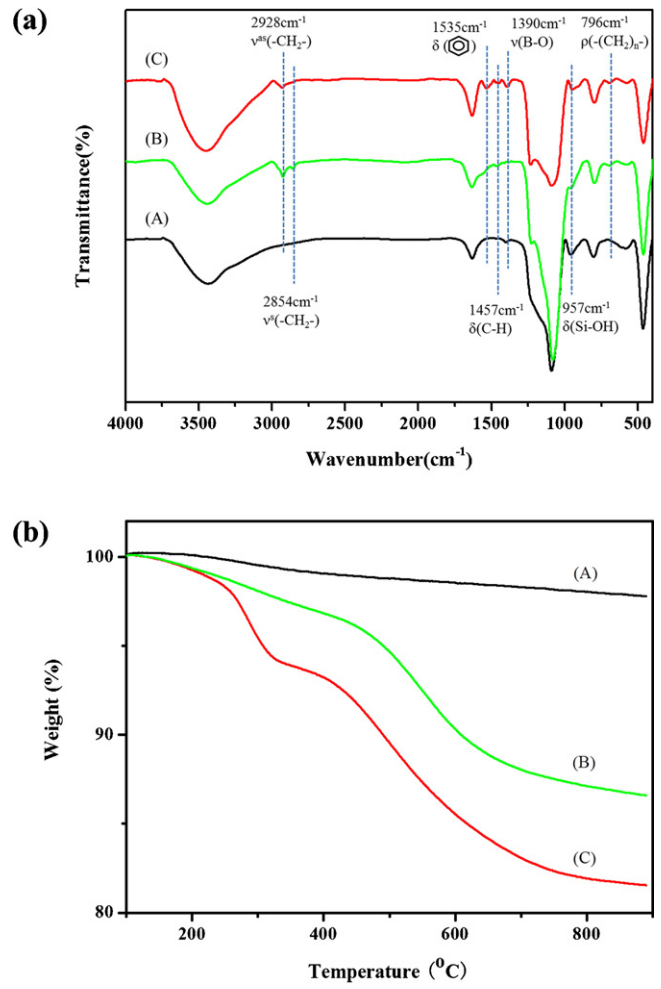

Fig. 2. (a) IR spectra of (A) MCM-41, (B) MCM-41-APTES, and (C) MCM-41-APTES-CPB; (b) TGA curves of (A) MCM-41, (B) MCM-41-APTES, and (C) MCM-41-APTES-CPB.

supporting information, Table S2). The pore volumes and specific surface areas of MCM-41-APTES and MCM-41-APTES-CPB gradually decreased by about 50% after each grafting step as a result of the organic layers bonded to the internal surface of MCM-41. The above results indicate that MCM-41-APTES-CPB still possesses the size-exclusion ability with a MW cutoff of 12 kDa. The appearance of the weak band of HRP in lane 12 may be caused by the boronic acid groups on the outside surface of MCM-41. In addition, the appearance of the weak bands of SBTI and Myo in lane 12 may be attributed to the electrostatic adhesion between these two proteins and the outside surface of MCM-41. These two proteins possess negative charges under the enrichment condition. The zeta potential (+42.7 mV) of MCM-41-APTES-CPB indicates its positive charge. Hence, they are partially adsorbed on the outside surface of MCM-41-APTES-CPB. However, this non-specificity does not seriously interfere with the subsequent glycopeptides capture as described below. The high in-pore surface area (ca. 95%) of MCM-41 ensures high-selectivity enrichment by preventing the adsorption of proteins on the inside surface of pores.

3.4. Selective enrichment efficiency of MCM-41-APTES-CPB for glycopeptides

The specificity for glycopeptides of the boronic acid-functionalized MCM-41 silica was compared to the unmodified counterpart MCM-41 (see supporting information, Fig. S1). Without enrichment, there was no signal of glycopeptides detected (Fig. S1a and b). After enrichment, Fig. S1c and d shows that seven dominant peaks of the standard glycoprotein HRP digest (asterisks represent fragments of glycopeptides, with *m/z* values of 1842, 2591, 3353, 3673, 3896, 4223 and 4986, respectively) are successfully observed. The *m/z* values of 1842, 2591, 3353, 3673, 3896, 4223 and 4986 can be attributed to these glycopeptides $Hex_3HexNAc_2dHex_1Pent_1$ (184–189) at N_{188}, $Hex_3HexNAc_2dHex_1Pent_1$ (225–236) at N_{216} and N_{228}, $Hex_3HexNAc_2dHex_1Pent_1$ (295–313) at N_{298}, $Hex_3HexNAc_2dHex_1Pent_1$ (272–294) at N_{285}, $Hex_3HexNAc_2dHex_1Pent_1$ (69–92) at N_{87}, $Hex_3HexNAc_2dHex_1Pent_1$ (31–49; 115–123) at N_{43} as well as $Hex_3HexNAc_2dHex_1Pent_1$ (214–236) at N_{216} and N_{228}, respectively [42,53]. However, there is no glycopeptides specifically enriched by MCM-41 and MCM-41-APTES (Fig. S1e–h).

Tryptic digests of the standard glycoprotein HRP and the standard non-glycoprotein BSA were used to investigate the enrichment efficiency of MCM-41-APTES-CPB for glycopeptides. The excellent selectivity of this approach was demonstrated by analyzing glycopeptides in the digest mixture of HRP and BSA with a molar ratio of 1:100 before (Fig. 4c and d) and after (Fig. 4a

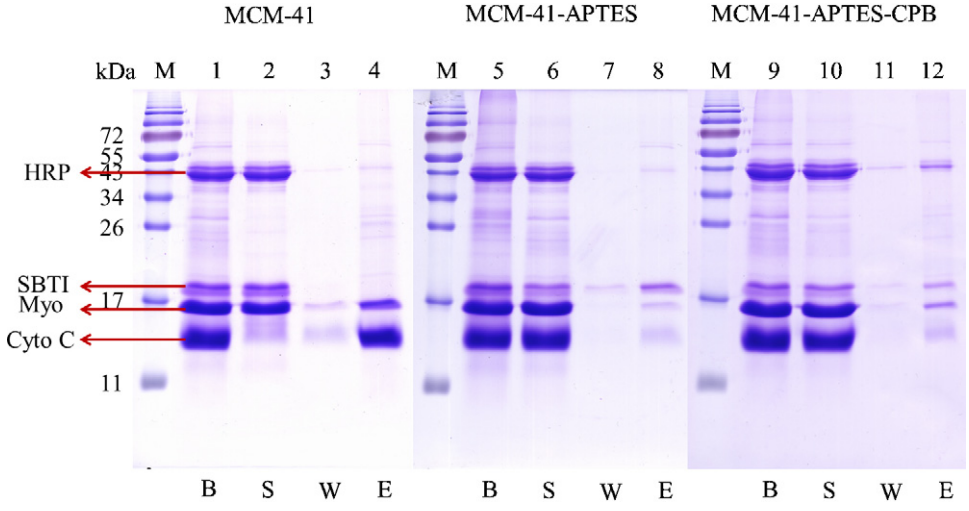

Fig. 3. Size-exclusion effect of unmodified and modified MCM-41 by SDS-PAGE separation of standard protein mixtures (HRP, SBTI, Myo and Cyto C). Lanes 1, 5, 9 (labeled as B) are the results before adsorption. Lanes 2–4; lanes 6–8; lanes 10–12 are the results after adsorption with MCM-41, MCM-41-APTES and MCM-41-APTES-CPB respectively. Lanes 2, 6, 10; lanes 3, 7, 11 and lanes 4, 8, 12 are the supernatants (labeled as S), washings (labeled as W) and elutions (labeled as E) after adsorption respectively.

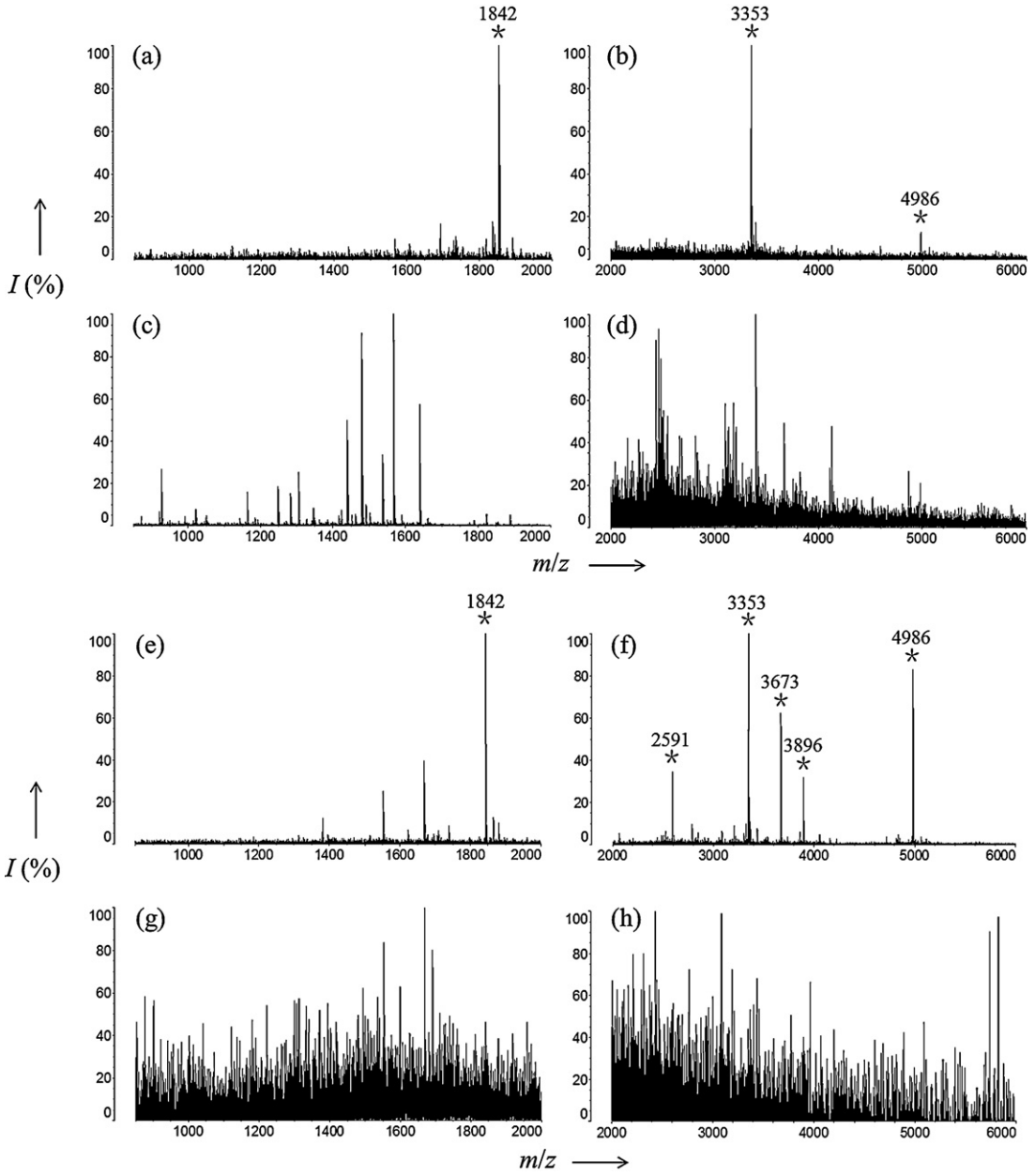

Fig. 4. MALDI-TOF mass spectra of tryptic BSA and HRP mixtures after (a, b) and before (c, d) enrichment at a molar ratio of 100:1; MALDI-TOF mass spectra of the tryptic HRP spiked rat serum with enrichment by MCM-41-APTES-CPB (e, f) and before enrichment (g, h). *HRP glycopeptide. (a, c, e, g) are the *m*/*z* ranges between 850 and 2000. (b, d, f, h) are the *m*/*z* ranges between 2000 and 6000.

and b) enrichment by MCM-41-APTES-CPB. Before enrichment, the glycopeptides are difficult to be distinguished because of the presence of large amounts of non-glycopeptides from BSA before enrichment (Fig. 4c and d). After the enrichment by MCM-41-APTES-CPB, three dominant peaks of glycopeptides (asterisks represent fragments of glycopeptides, with *m*/*z* values of 1842, 3353, and 4986, respectively) are successfully observed with a clean background at the optimized enrichment condition. The selectivity of this method is one of the highest selectivity reported so far. For example, although the latest reported selectivity for glycoprotein of the teamed boronate affinity-functionalized Fe_3O_4@Au core/satellite magnetic nanoparticles is also at a molar ratio of glycoprotein/non-glycoprotein of 1:100, the glycoprotein RNase B could be hardly detected [54]. To further evaluate the sensitivity of MCM-41-APTES-CPB for glycopeptide enrichment, the glycopeptide at *m*/*z* = 2591 was used to determine the limit of detection (LOD) at a signal/noise (S/N) of 3 (see supporting information, Fig. S2). The S/N was 14 when the concentration of tryptic HRP was 5 fmol μL^{-1}. Assuming that there was a linear relationship between the concentration of tryptic HRP and the S/N, as a result, LOD was calculated to be as low as 1 fmol μL^{-1} and experimentally lower than 5 fmol μL^{-1}. The lowest LOD of tryptic HRP reported so far was 0.62 fmol μL^{-1} [42] and the LOD of our method is also at the fmol level, which indicates the high sensitivity of this method. The binding capacity of the MCM-41-APTES-CPB was also determined to be 40 mg g^{-1} (see supporting information, Fig. S3).

The post-enrichment recovery of glycopeptides from MCM-41-APTES-CPB was investigated. A certain amount (2 μg) of tryptic HRP was equally divided into two parts. The first part was treated with trypsin in $H_2{}^{18}O$, which produced a 4 Da mass increase by

Table 1
The identified endogenous glycopeptides in rat serum by using MCM-41-APTES-CPB with nano LC–MS/MS analysis.

Precursor protein	Peptide sequence	MH^+	z	pI
Lysosomal acid phosphatase	F.LDMVAN#ETGLMN^L.T	1422.616	2	3.67
Acyl-protein thioesterase 1	T.LN#MSM*M*M.P	890.3088	2	5.52
Aa2-050	S.NNSNNKNSNN#NSNNN.N	1663.671	2	8.75
Proprotein convertase subtilisin/kexin type 5	K.GN#ATSCHSC.E	880.3016	2	6.72
Tudor domain-containing protein 7	A.SSPGN^RN#AST.P	992.3972	2	9.47
rCG31851, isoform CRA_b/a	H.FGLEEPN#FSLA.Y	1224.579	2	3.79
Microfibrillar-associated protein 3-like	L.ATAKSVTN#STLNGTDVVL.G	1791.962	2	5.88
Sulphonylurea receptor 2b	T.SN#LSMGEM*TLGQIN^.N	1512.669	2	4.00
Janus kinase 1	S.SENELSRCHSN#DSGNV.L	1748.728	2	4.65
Glutamate carboxypeptidase 2	Y.INADSSIEGN#YTLR.V	1553.738	3	4.37
RCG51979	F.TRGN#MTRM*VEDA.I	1397.634	2	5.74
PREDICTED: hypothetical protein	E.N#N^SDDN^RVNICPDN.Y	1592.631	2	3.93
PREDICTED: ubiquitination factor E4B	L.NLLLVLKYN#LTV.P	1403.869	2	8.59
PREDICTED: rCG52155-like	I.ALLLLKSPLN#LSINGIPICTS.E	2181.292	3	8.27
PREDICTED: zinc finger protein 53-like	L.VN#STITVTAEVYGM*YNPNN^.I	2104.943	2	4.00

N#: N-linked glycosylation site; N^: deamidation of N transformed into D; M*: oxidation of methionine.

introducing two ^{18}O atoms at the C-termini of the peptides, and applied in our glycopeptide enrichment strategy. The second part was treated with trypsin in H_2O. By mixing the two parts, we could profile the product with MS to make a comparative study of the abundances of the glycopeptides from different oxygen isotopes, according to the peak relative intensities [55,56]. A mixture of ^{18}O-labeled unenriched and an equal amount of unlabeled unenriched was used as a control. As the MALDI-TOF spectra reveal (see supporting information, Fig. S4), the post-enrichment recovery of glycopeptides is up to 88.10% calculated according to the isotope distribution (based on relative intensity), which is the highest recovery reported so far when compared to the recovery of the latest reported is 85.9% [38].

The careful design of the structure and synthetic route provides the MCM-41-APTES-CPB with an excellent specificity and additional advantages for the enrichment of glycopeptides. The post-grafting method adopted to introduce boronic acid groups (B concentration is 33.56×10^{-5} mol g^{-1}) efficiently leads to a large internal surface with abundant glycopeptide-binding sites (binding capacity is 40 mg g^{-1}). Therefore, glycopeptides could be easily enriched with high selectivity (molar ratio of glycopeptides/non-glycopeptides is 1:100) and efficiency (LOD is at fmol level) once they enter the pores. In addition, the reversible reaction can also readily and efficiently recover the captured glycopeptides under mild conditions for further analysis (recovery is up to 88.10%). In fact, the capture and release of glycopeptides can be easily controlled by adjusting the pH of solution from weakly alkaline (pH 8) to acidic (pH 3) using TEA and TFA without adding any nonvolatile agent that may interfere with detection. MCM-41-APTES-CPB is expected to be an outstanding adsorbent for profiling serum glycopeptidome due to its excellent size-exclusion and glycopeptide-enrichment abilities. Therefore, to confirm this expectation, tryptic digest of HRP was spiked into rat serum and an enrichment experiment was carried out to determine whether MCM-41-APTES-CPB could extract the glycopeptides from these mixed serum samples. The MALDI-TOF mass spectra of the HRP digest spiked serum samples before (Fig. 4g and h) and after (Fig. 4e and f) enrichment by MCM-41-APTES-CPB were obtained. Fig. 4(e and f) show that six dominant peaks of the HRP digest (asterisks represent fragments of glycopeptides, with m/z values of 1842, 2591, 3353, 3673, 3896, and 4986, respectively) are successfully observed with a clean background. However, there is no glycopeptide detected without enrichment (Fig. 4g and h). Therefore, the boronic acid-functionalized MCM-41 silica could effectively enrich glycopeptides from a complex biological sample, thereby establishing the foundation for the research of the serum glycopeptidome.

3.5. Profiling of rat serum glycopeptidome by MCM-41-APTES-CPB

The proposed boronic acid-functionalized mesoporous silica-based enrichment method has been proven to be effective for the profiling of endogenous glycopeptides in rat serum samples. The procedure for the extraction of serum endogenous glycopeptides using MCM-41-APTES-CPB is illustrated in Scheme 1(b). 1.0 mL of rat serum was diluted by 2.0 mL of ACN and denatured by heating. Subsequently, 10.0 mg of MCM-41-APTES-CPB was added to enrich the glycopeptides. The enriched glycopeptides were released and deglycosylated by PNGase F, separated by nano-LC, and fragmented by MS/MS using an ESI-LTQ Orbitrap instrument. A total of 15 glycopeptides and their 15 corresponding glycosites (with N-X-S/T (X ≠ P) sequences) were identified via a database search (Table 1). A representative MS/MS spectrum of the glycopeptide N#NSDDNRVNICPDN identified by CID fragmentation using an LTQ Orbitrap instrument is shown (see supporting information, Fig. S5). The combination of the mass increment of 0.98402 Da of asparagine (N) transforms into aspartic acid (D), and the existence of N-X-S/T sequences clearly and definitely identifies the glycopeptides and glycosites [57]. The MWs of the deglycosylated glycopeptides are all below 2500 Da, and the pI ranges are between 3 and 10. These glycopeptides and their corresponding glycosites are all newly discovered in this study. These identified glycopeptides and the corresponding precursor proteins are also shown in Table 1. These glycopeptides might be endogenously-generated peptides or some cleavages from the processes of protein degradation. The revelation of these glycopeptides may provide more information on biological processes. For instance, the precursor of the glycopeptide F.LDMVAN#ETGLMNL.T is lysosomal acid phosphatase, which is a glycoprotein located at the lysosome membrane with the molecular function of being a hydrolase, as well as being related to some biological processes, such as autophagic cell death, response to organic substance, and synaptic transmission [58].

4. Conclusion

In summary, a highly ordered boronic acid-functionalized mesoporous silica (MCM-41-APTES-CPB) was synthesized using a post-grafting method. MCM-41-APTES-CPB was successfully applied in the enrichment of endogenous glycopeptides in rat serum samples. The size-exclusion effect of unique mesoporous structures and the abundant boronic acid groups covering the internal surface confer the superior ability for endogenous glycopeptide enrichment. As a result of the easy and effective procedure for the extraction, release, and identification of glycopeptides,

this technology for revelation of serum glycopeptidome using boronic acid-functionalized mesoporous silica is believed to be very promising for the highly specific discovery of serum endogenous glycopeptides as potential biomarkers for clinical diagnoses.

Acknowledgements

The work was supported by NST (2012CB910602 and 2012AA020203), NSF (21025519 and 21005020, 31070732), Shanghai Projects (11XD1400800, Shuguang, Eastern Scholar, B109 and 20114Y167).

Appendix A. Supplementary data

Supplementary data associated with this article can be found, in the online version, at http://dx.doi.org/10.1016/j.aca.2012.10.002.

References

[1] P. Schulz-Knappe, H.D. Zucht, G. Heine, M. Jürgens, R. Hess, M. Schrader, Comb. Chem. High Throughput Screening 4 (2001) 207–217.
[2] M. Schrader, P. Schulz-Knappe, Trends Biotechnol. 19 (2001) S55–S60.
[3] V.T. Ivanov, O.N. Yatskin, Expert Rev. Proteomics 2 (2005) 463–473.
[4] L. Hu, M. Ye, H. Zou, Expert Rev. Proteomics 6 (2009) 433–447.
[5] E.F. Petricoin, A.M. Ardekani, B.A. Hitt, P.J. Levine, V.A. Fusaro, S.M. Steinberg, G.B. Mills, C. Simone, D.A. Fishman, E.C. Kohn, L.A. Liotta, Lancet 359 (2002) 572–577.
[6] L.A. Liotta, M. Ferrari, E. Petricoin, Nature 425 (2003) 905.
[7] J. Villanueva, D.R. Shaffer, J. Philip, C.A. Chaparro, H. Erdjument-Bromage, A.B. Olshen, M. Fleisher, H. Lilja, E. Brogi, J. Boyd, M. Sanchez-Carbayo, E.C. Holland, C. Cordon-Cardo, H.I. Scher, P. Tempst, J. Clin. Invest. 116 (2006) 271–284.
[8] K. Sasaki, Y. Satomi, T. Takao, N. Minamino, Mol. Cell. Proteomics 8 (2009) 1638–1647.
[9] J. Villanueva, A.J. Martorella, K. Lawlor, J. Philip, M. Fleisher, R.J. Robbins, P. Tempst, Mol. Cell. Proteomics 5 (2006) 1840–1852.
[10] M.F. Lopez, A. Mikulskis, S. Kuzdzal, E. Golenko, E.F. Petricoin III, L.A. Liotta, W.F. Patton, G.R. Whiteley, K. Rosenblatt, P. Gurnani, A. Nandi, S. Neill, S. Cullen, M. O'Gorman, D. Sarracino, C. Lynch, A. Johnson, W. Mckenzie, D. Fishman, Clin. Chem. 53 (2007) 1067–1074.
[11] K. Sköld, M. Svensson, M. Norrman, B. Sjögren, P. Svenningsson, P.E. Andrén, Proteomics 7 (2007) 4445–4456.
[12] L. Hu, H. Zhou, Y. Li, S. Sun, L. Guo, M. Ye, X. Tian, J. Gu, S. Yang, H. Zou, Anal. Chem. 81 (2009) 94–104.
[13] Y. Hu, Y. Peng, K. Lin, H. Shen, L.C. Brousseau III, J. Sakamoto, T. Sun, M. Ferrari, Nanoscale 3 (2011) 421–428.
[14] K. Ohtsubol, J.D. Marthl, Cell 126 (2006) 855–867.
[15] J.N. Adkins, S.M. Varnum, K.J. Auberry, R.J. Moore, N.H. Angell, R.D. Smith, D.L. Springer, J.G. Pounds, Mol. Cell. Proteomics 1 (2002) 947–955.
[16] G. Alvarez-Manilla, J. Atwood III, Y. Guo, N.L. Warren, R. Orlando, M. Pierce, J. Proteome Res. 5 (2006) 701–708.
[17] A. Khan, N.H. Packer, J. Proteome Res. 5 (2006) 2824–2838.
[18] R.S. Tirumalai, K.C. Chan, D.A. Prieto, H.J. Issaq, T.P. Conrads, T.D. Veenstra, Mol. Cell. Proteomics 2 (2003) 1096–1103.
[19] J. Villanueva, J. Philip, D. Entenberg, C.A. Chaparro, M.K. Tanwar, E.C. Holland, P. Tempst, Anal. Chem. 76 (2004) 1560–1570.
[20] M. Gaspari, M.M. Cheng, R. Terracciano, X. Liu, A.J. Nijdam, L. Vaccari, E.D. Fabrizio, E.F. Petricoin, L.A. Liotta, G. Cuda, S. Venuta, M. Ferrari, J. Proteome Res. 5 (2006) 1261–1266.
[21] L. Hu, K. Boos, M. Ye, R. Wu, H. Zou, J. Chromatogr. A 1216 (2009) 5377–5384.
[22] Y. Liu, Y. Lu, Z. Liu, Chem. Sci. 3 (2012) 1467–1471.
[23] R. Tian, H. Zhang, M. Ye, X. Jiang, L. Hu, X. Li, X. Bao, H. Zou, Angew. Chem. Int. Ed. 46 (2007) 962–965.
[24] H. Qin, P. Gao, F. Wang, L. Zhao, J. Zhu, A. Wang, T. Zhang, R. Wu, H. Zou, Angew. Chem. Int. Ed. 50 (2011) 12218–12221.
[25] Z. Yang, W.S. Hancock, J. Chromatogr. A 1053 (2004) 79–88.
[26] J. Zhao, D.M. Simeone, D. Heidt, M.A. Anderson, D.M. Lubman, J. Proteome Res. 5 (2006) 1792–1802.
[27] R.R. Drake, E.E. Schwegler, G. Malik, J. Diaz, T. Block, A. Mehta, O.J. Semmes, Mol. Cell. Proteomics 5 (2006) 1957–1967.
[28] H. Zhang, X. Li, D.B. Martin, R. Aebersold, Nat. Biotechnol. 21 (2003) 660–666.
[29] M. Wuhrer, C.A.M. Koeleman, C.H. Hokke, A.M. Deelder, Anal. Chem. 77 (2005) 886–894.
[30] W. Ding, J.J. Hill, J. Kelly, Anal. Chem. 79 (2007) 8891–8899.
[31] L. Ren, Y. Liu, M. Dong, Z. Liu, J. Chromatogr. A 1216 (2009) 8421–8425.
[32] J. Tan, H. Wang, X. Yan, Anal. Chem. 81 (2009) 5273–5280.
[33] Y. Liu, L. Ren, Z. Liu, Chem. Commun. 47 (2011) 5067–5069.
[34] P. Dou, Z. Liu, Anal. Bioanal. Chem. 399 (2011) 3423–3429.
[35] H. Li, H. Wang, Y. Liu, Z. Liu, Chem. Commun. 48 (2012) 4115–4117.
[36] M. Chen, Y. Lu, Q. Ma, L. Guo, Y. Feng, Analyst 134 (2009) 2158–2164.
[37] Z. Lin, J. Zheng, F. Lin, L. Zhang, Z. Cai, G. Chen, J. Mater. Chem. 21 (2011) 518–524.
[38] L. Zhang, Y. Xu, H. Yao, L. Xie, J. Yao, H. Lu, P. Yang, Chem. Eur. J. 15 (2009) 10158–10166.
[39] W. Shen, C. Ma, S. Wang, H. Xiong, H. Lu, P. Yang, Chem. Asian J. 5 (2010) 1185–1191.
[40] D. Qi, H. Zhang, J. Tang, C. Deng, X. Zhang, J. Phys. Chem. C 114 (2010) 9221–9226.
[41] J. Tang, Y. Liu, D. Qi, G. Yao, C. Deng, X. Zhang, Proteomics 9 (2009) 5046–5055.
[42] Y. Xu, Z. Wu, L. Zhang, H. Lu, P. Yang, P. Webley, D. Zhao, Anal. Chem. 81 (2009) 503–508.
[43] F. Frantzen, K. Grimsrud, D.E. Heggli, E. Sundrehagen, J. Chromatogr. B 670 (1995) 37–45.
[44] L. Ren, Z. Liu, Y. Liu, P. Dou, H. Chen, Angew. Chem. Int. Ed. 48 (2009) 6704–6707.
[45] J. Fan, C. Yu, F. Gao, J. Lei, B. Tian, L. Wang, Q. Luo, B. Tu, W. Zhou, D. Zhao, Angew. Chem. Int. Ed. 42 (2003) 3146–3150.
[46] Y. Han, S.S. Lee, J.Y. Ying, Chem. Mater. 18 (2006) 643–649.
[47] S.B. Hartono, S.Z. Qiao, K. Jack, B.P. Ladewig, Z. Hao, G.Q. Lu, Langmuir 25 (2009) 6413–6424.
[48] H.H.P. Yiu, P.A. Wright, J. Mater. Chem. 15 (2005) 3690–3700.
[49] M. Hartmann, D. Jung, J. Mater. Chem. 20 (2010) 844–857.
[50] Y. Zhao, B.G. Trewyn, I.I. Slowing, V.S. Lin, J. Am. Chem. Soc. 131 (2009) 8398–8400.
[51] J.E. DeLorbe, J.H. Clements, M.G. Teresk, A.P. Benfield, H.R. Plake, L.E. Millspaugh, S.F. Martin, J. Am. Chem. Soc. 131 (2009) 16758–16770.
[52] J.S. Gelman, J. Sironi, L.M. Castro, E.S. Ferro, L.D. Fricker, J. Proteome Res. 10 (2011) 1583–1592.
[53] M. Wuhrer, C.H. Hokke, A.M. Deelder, Rapid Commun. Mass Spectrom. 18 (2004) 1741–1748.
[54] L. Liang, Z. Liu, Chem. Commun. 47 (2011) 2255–2257.
[55] X. Yao, A. Freas, J. Ramirez, P. Demirev, C. Fenselau, Anal. Chem. 73 (2001) 2836–2842.
[56] L. Zang, D. Toy, W. Hancock, D. Sgroi, B. Karger, J. Proteome Res. 3 (2004) 604–612.
[57] X. Liu, L. Ma, J. Li, Anal. Lett. 41 (2008) 268–277.
[58] M. Himeno, H. Fujita, Y. Noguchi, A. Kono, K. Kato, Biochem. Biophys. Res. Commun. 162 (1989) 1044–1053.